ACS Energy LETTERS

http://pubs.acs.org/journal/aelccp

Comparing Advanced Bipolar Membranes for High-Current Electrodialysis and Membrane Electrolysis

Olivia T. Vulpin, James B. Mitchell, Lihaokun Chen, Jeonghoon Lim, Sayantan Sasmal, Nathan G. Price, Sam R. Jarvis, and Shannon W. Boettcher*

Cite This: *ACS Energy Lett.* 2025, 10, 845−852

Read Online

ACCESS | Metrics & More | Article Recommendations | Supporting Information

ABSTRACT: Advanced bipolar membranes (BPMs) with low water-dissociation overpotential (η_{wd}) may enable new electrochemical technologies for electrolysis, fuel cells, acid−base synthesis, brine remediation, lithium-battery recycling, and cement production. However, these advanced BPMs have only been demonstrated in BPM water electrolysis (BPMWE) configurations where the BPM is under static compression by the porous-transport layers. It is important to study these BPMs in applications like electrodialysis where large degrees of static compression are not possible. We present a BPM electrodialysis (BPMED) platform to measure water-dissociation overpotential (η_{wd}) and compare BPMWE and BPMED systems. We show advanced BPMs with half the η_{wd} compared to commercial BPMs for BPMED while maintaining ∼90% current efficiency from 0.05−0.5 A cm^{-2}. The BPMED η_{wd} values are, however, about 0.2 V higher at 0.5 A cm^{-2} than those for BPMWE. Regardless, these results show that BPMs developed and optimized in BPMWE applications are well-suited for next-generation high-current-density BPMED technologies.

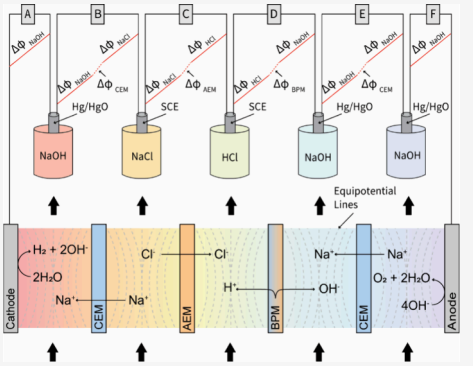

Bipolar membranes (BPMs) are composed of a polymeric anion-exchange layer (AEL) and cation-exchange layer (CEL) sandwiched together around a catalytic layer that speeds water dissociation (Figure 1a). These polymers are ionomers composed typically of a hydrophobic backbone functionalized with stationary charged groups, such as sulfonic acid groups for the CEL and quaternary ammonium groups for the AEL.[1] Ion-exchange layers conduct ions with opposite sign (counterions) to those of the charged groups bound to the backbone and exclude ions of the same sign (co-ions). With these differently charged layers, the BPM is able to maintain large pH gradients via water dissociation at the junction of the CEL and AEL, making them useful for a broad range of applications, such as electrolyzers, fuel cells, desalination, acid−base production, brine remediation, and lithium recovery, among others.[2−6] Broadly, these technological applications fall into two categories−those where electrolytes freely flow on either side of the BPM, such as in electrodialysis (Figure 1c) and those where the BPM is part of a membrane-electrode assembly, such as in an electrolyzer or fuel cell, and compressed under high static pressure via a rigid porous-transport layer and where the electrolyte flows along the electrodes, not interfacing directly with the BPM (Figure 1b).

Membrane-electrode assemblies have become a primary test platform for understanding the mechanisms governing the function of BPMs, and consequently the platform that has seen the most advancement in BPM technology. BPM-containing membrane-electrode assemblies provide a system where the only mobile ions are H^+ and OH^-, unlike BPM electrodialysis systems where a range of mobile ions are present depending on the supporting electrolytes, complicating models and electrochemical analysis. Furthermore, membrane-electrode assemblies hold the BPM under spatially even, static compression, which has been shown to impact performance of the ionomer layers making up the BPM, while the freely flowing electrodialysis applications for BPM are generally unable to provide consistent static pressure to the BPM.[7−9]

The ionic resistance of the BPM can be broken into two parts, the resistance of the membrane layers (CEL and AEL)

Received: December 22, 2024
Accepted: January 9, 2025
Published: January 18, 2025

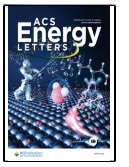

Downloaded via UNIV OF OREGON on September 22, 2025 at 21:21:08 (UTC).
See https://pubs.acs.org/sharingguidelines for options on how to legitimately share published articles.

ACS Publications © 2025 American Chemical Society

https://doi.org/10.1021/acsenergylett.4c03538
ACS Energy Lett. 2025, 10, 845−852

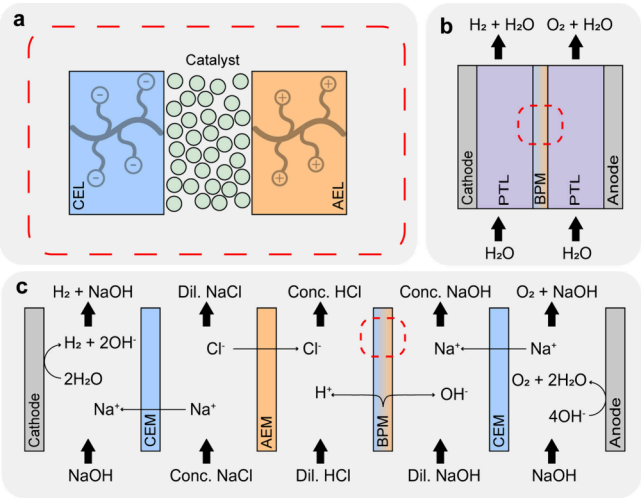

Figure 1. (a) Expanded view of the BPM with catalyst, cation-exchange layer (CEL), and anion-exchange layer (AEL) labeled with schematic polymer structures. (b) Bipolar membrane (BPM) electrolyzer (BPMWE) schematic including rigid porous-transport layers (PTLs). (c) BPM electrodialysis (BPMED) schematic showing the additional cation-exchange (CEM) and anion-exchange (AEM) membranes used in a single-cell test system.

and the water dissociation (WD, $H_2O \rightarrow H^+ + OH^-$) resistance, which can be equivalently cast as the WD overpotential (η_{wd}) as a function of current. To address membrane layer resistance, diverse polymer structures have been proposed and synthesized to reduce counterion transport resistance through the membrane, while assuring that adequate co-ion selectivity of the membrane is maintained for a given application.[10,11] Similarly, researchers have focused on understanding the mechanisms that underly the measured η_{wd} within the BPM to inform WD catalyst designs.[12,13] Historically, η_{wd} was the largest source of voltage inefficiency in the BPM, but this is now changing due to the introduction of advanced WD catalyst designs that dramatically speed the WD reaction within the BPM.[14−17]

The precise molecular mechanisms of WD within these BPM junctions remain unsettled. Initial theories around "WD catalysis" arose from the hypothesis that weakly basic tertiary amino groups on the AEL near the BPM junction could accept and donate protons as an intermediate step in the WD reaction.[14] Recently, the BPM water electrolysis (BPMWE) architecture, where the only mobile ions are H^+ and OH^-, has been used to understand the WD reaction and to test and improve new WD catalysts, practically leading to >20× reduction in η_{wd}.[18] The acid−base properties of metal-oxide nanoparticles in the BPM junction are thought to be important for catalyst bilayers, as evidenced by the connection between the pH of zero charge on the metal-oxide and the local pH near the AEL, or CEL, in the BPM.[12] The impact of interfacial electric field is also important; adding noncatalytic electronically conductive carbon particles at the BPM junction increases the rate of WD perhaps by focusing the electric field at the interfaces where WD occurs.[10,19−21] In the above cases, the introduced WD catalysts are typically in the form of metal-oxide nanoparticles and are applied to the junction between the two layers of the BPM without supporting ionomer or other polymer adhesive, likely in part leading to the high performance.[10,12,22]

One limitation of much of the work on advanced catalyzed BPM is that they have been studied in the BPMWE platform where the BPM is under static compression in the membrane-electrode assembly (MEA) and fed pure water. As compared to a BPM in applications like electrodialysis, where the BPM is exposed to a wide range of free-flowing electrolytes, leading to possible ion contamination and low static pressure holding the BPM together. Here we study how advanced BPMs, with excellent BPMWE performance in MEAs, operate in a BPM electrodialysis (BPMED) stack.

BPMED is a technology that produces acid and base from brine (salt) solution (Figure 1c). Historically, the design of BPMED systems have emphasized the production of high-concentration and high-purity solutions, with little focus on the energy efficiency.[23−25] Thus, BPMED systems have generally used higher-resistance membranes that have good selectivity and can withstand high-concentration solutions without significant co-ion leakage. However, this means that these systems have low energy efficiency, especially when driven at higher currents, in exchange for high current efficiency. Further, the BPMs used in BPMED systems have not seen dramatic development since their implementation at the industrial level in the 1960s.[25,26]

BPMED systems can be configured with a wide range of electrolyte and membrane orientations, expanding their uses to applications including CO_2 capture, water purification, lithium and other metals separation and recovery, and even cement-clinker production.[4−6,27,28] Most of these applications are at the lab-scale, with some recently emerging at the pilot-scale. The slow commercialization and scaling of these systems is in part due to the inefficiency of conventional BPMs.[6] With the introduction of advanced BPMs into BPMED systems, the energy efficiency of the system should increase, allowing for higher current-density and increased product production rate which significantly lower capital costs of emerging BPMED and related technologies.

The construction of the BPMED and pure-water BPM electrolysis systems are related but differ in several important ways. For the BPMWE system, the BPM is subject to high and even internal pressure due to the catalyst and porous-transport layers (Figure 1b).[9,29] These porous-transport layers are typically made up of multiple packed nickel, steel, or titanium-woven fiber layers, or porous carbon, resulting in a relatively uniform surface. The BPMWE protocols used in this study, and for others from our team, were adopted from proton-exchange-membrane (PEM) electrolyzers.[12] For PEM electrolyzers, increased compression enhances electrolyzer performance because of improved contact between the electrically conductive porous-transport layers and the ionically conductive membrane.[30,31] However, if compression is too high, water transport through the PEM electrolyzer membrane is impeded and the system resistance increases.[32] Despite the impacts of compression on PEM electrolyzer performance, there is little documented on the impact of compression on the BPM. This is interesting when using BPMs in BPMED systems that can provide a range of internal pressures as the spacers and materials used in the BPMED flow fields are changed (Figure S1). Within the BPMED system, flow-field spacers are typically course, single-layer weaves of inert plastic, such as polypropylene, with weave wire diameters ranging from ∼100 μm to 1 mm and thus lead to uneven compression on the membrane surface.[24,33,34] More broadly, little is known about the ideal compression of the BPMs in BPMED systems with

https://doi.org/10.1021/acsenergylett.4c03538
ACS Energy Lett. 2025, 10, 845−852

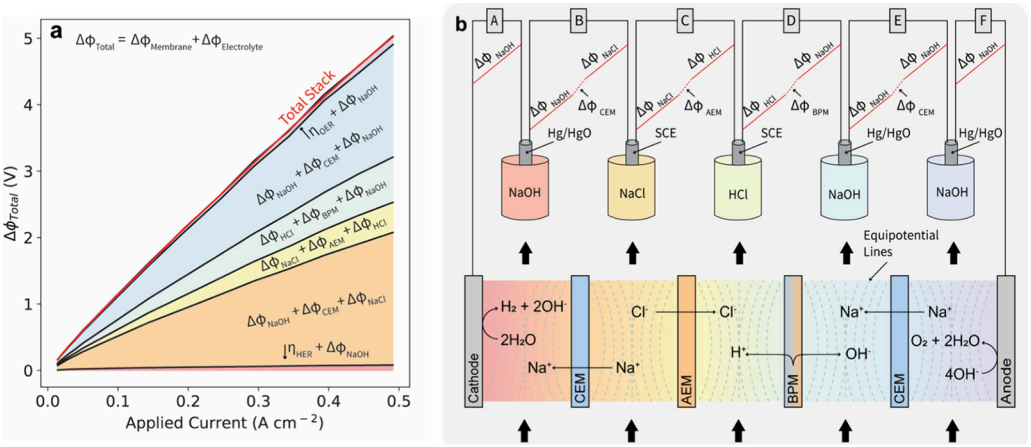

Figure 2. (a) Overpotential across each measured circuit throughout the BPM electrodialysis (BPMED) system (i.e., potential change as a function of current, relative to the open-circuit value), totaling to the measured entire system voltage (total stack) at 25 °C. (b) Schematic of the membrane and electrolyte layers in the BPMED stack, with the different measured potential drop circuits labeled A through F and schematic potential drops ($\Delta\phi$) within each circuit. The $\Delta\phi$ values from the center of one flow channel, across a membrane, and to the center of an adjacent flow channel are measured using reference electrodes in the reservoirs feeding each electrolyte flow of the overall stack. The color gradients schematically represent the potential gradients in each section of the electrodialysis stack. We take each reservoir (represented as the uniform-colored cylinders) as equipotential to the electrolyte at approximately the midpoint of the flow channel represented by the vertical dashed line. An ohmic potential drop is present across the electrolyte region and the membrane region of the system. The measured steady-state voltage changes also include contributions from concentration polarization in addition to contributions from electric-potential drops driving migration. Circuits A and F further include the reaction kinetic overpotentials which are not important in this study but contribute to the overall cell voltage.

regards to membrane performance, which relies heavily on the details of the BPM junction and membrane fabrication.[34−36]

In addition to the different possible effects of static pressure on the BPM, there are differences in degradation and fouling mechanisms present in BPMED compared to BPMWE. BPMWE is often run with pure water contacting the BPM surface, while in BPMED the BPM is exposed to a range of differential electrolyte concentrations, compositions, and pHs. As the concentration of the solution contacting the AEL and/or CEL making up the BPM increases, the membrane is less able to exclude the transport of co-ions (via Donnan exclusion) through the respective layers.[37,38] The unwanted transport of co-ions may lead to fouling of the catalyst at the BPM junction, contamination of adjacent solutions, shunt currents, and surface contamination of the BPM as divalent ions precipitate at the BPM surface.

With these differences in mind, we report a lab-scale BPMED platform suitable for the study of potential drops throughout the BPMED system via the introduction of reference electrodes to the brine, acid, base, and electrolyte feed solutions (Figure 2b). This platform enables the measurement of parameters such as η_{wd} to compare directly between the BPMWE and BPMED systems. We find that the new metal-oxide WD catalysts developed for use in BPMWE substantially lower the transmembrane voltage at a given current, due to lower η_{wd}, in the BPMED systems. The absolute η_{wd}, however, in the BPM electrodialysis devices are roughly twice that of the equivalent WD catalyst in the BPMWE devices at equivalent temperatures. These results are important because they demonstrate that the fundamental principles governing the performance of WD catalysts in advanced BPMs in the BPMWE system translate to the BPMED platform, despite the BPMED platform having co-ions present and a lower static pressure.

We also report current efficiency data for the advanced BPMs in BPMED compared to commercial Fumasep BPM. Although the advanced BPMs were constructed with AEL and CEL designed for fuel cells and electrolyzers that typically have high $H^+$and OH^-ion conductivity, but lower permselectivity, current efficiency values were found to be on par with commercial Fumasep BPM. The good current efficiency found in the advanced BPMED system, particularly at the larger WD currents studied, may be due to the high efflux of and ions preventing the influx of unwanted co-ions.[39] These findings thus demonstrate the feasibility of high current, next-generation BPMED stacks. With appropriate system engineering, these membranes may lower capital expenses by increasing the generation rate per area of acid and base for a variety of applications in water treatment, separations, and carbon-dioxide capture.

HIGH-CURRENT BPM ELECTRODIALYSIS TEST CELL DESIGN AND OPERATION

A BPMED test cell was designed with several degrees of adjustability and monitoring capabilities to aid in understanding the BPMED system. This approach allows for the overall BPMED system to be broken down into six different circuits that record the potential drop across specific features of the BPMED system (Figure 2). To record these individual circuits, reference electrodes were placed in the external solution reservoirs feeding the respective five solutions circulating through the BPMED system. Because current does not pass through the electrolyte in the tubing connecting the cell to the reservoirs, these are taken to be roughly equipotential and at an electric potential that is approximately equal to the average electric potential of the electrolyte flowing through the spacer-filled flow-field medium between each set of membranes.

Given this measurement scheme and approximation for electric-potential breakdown, the total potential changes relative to the open-circuit value, as a function of current, can be further broken down into their electrolyte, membrane,

https://doi.org/10.1021/acsenergylett.4c03538
ACS Energy Lett. 2025, 10, 845−852

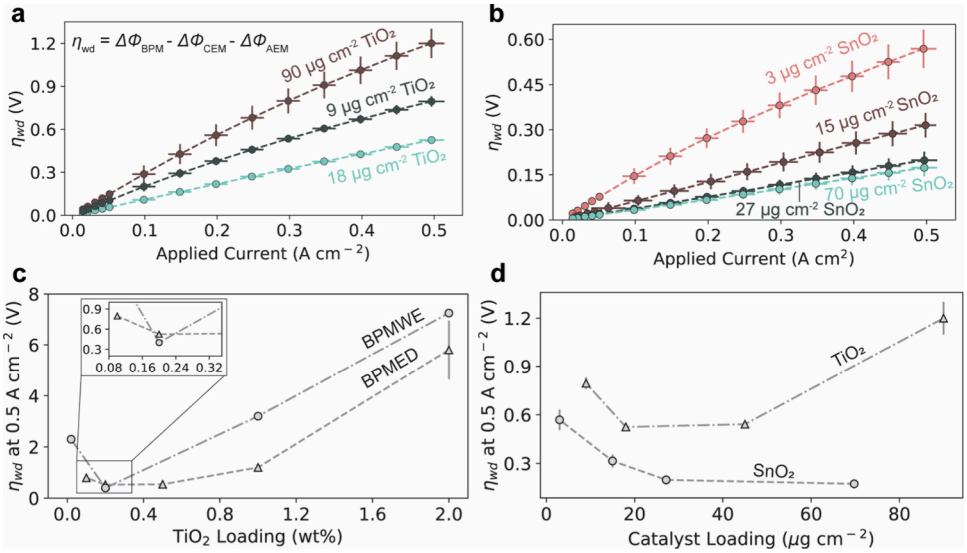

Figure 3. Effect of catalyst type and loading. (a) Polarization curve showing η_{wd} in the BPMED system with TiO_2 WD catalyst loading varied. (b) Polarization curve depicting η_{wd} in the BPMED system as SnO_2 nanoparticle catalyst loading is varied. (c) The η_{wd} at 0.5 A cm^{-2} as TiO_2 catalyst loading is varied for BPM water electrolysis (BPMWE; circle) and BPMED (triangle) systems. (d) The η_{wd} at 0.5 A cm^{-2} as catalyst loading for TiO_2 and SnO_2 is varied for the BPMED system. All BPMED and BPMWE runs were collected at 25 °C in triplicate, and error bars are shown as one standard deviation in cases where they are larger than the symbols.

or reaction overpotentials, depending on the circuit measured (Figure 2b). Of particular interest to this study is circuit D, which contains the BPM, and thus the contribution of η_{wd}. Circuit D can be broken down into the overpotential across the BPM ($\Delta\phi_{BPM}$), the acid solution ($\Delta\phi_{HCl}$), and the base solution ($\Delta\phi_{NaOH}$).

$$\Delta\phi_{total,D} - \Delta\phi_{total,D,OCV} = \Delta\phi_{BPM} + \Delta\phi_{HCl} + \Delta\phi_{NaOH} \quad (1)$$

Note that terms $\Delta\phi_{HCl}$ and $\Delta\phi_{NaOH}$ each represent one-half of the total electric-potential drop across the flowing electrolyte regions, and that the open-circuit potential (OCV) for this circuit is subtracted from the total potential. The potential drops $\Delta\phi_{HCl}$ and $\Delta\phi_{NaOH}$ can be calculated from

$$\Delta\phi = iR \quad (2)$$

The resistance (R) is calculated from the known conductivity (κ), length (l, along the current path), and A the area of the electrolyte flow channel.

$$R = \frac{1}{\kappa} \times \frac{l}{A} \quad (3)$$

To calculate the resistance of the electrolyte solutions (HCl and NaOH) in circuit D and the contributions of $\Delta\phi_{HCl}$ and $\Delta\phi_{NaOH}$, κ for each is calculated from the ion concentrations of each solution and the reported molar conductivities.[40] It was assumed that the reference electrodes were equipotential with the electrolyte exactly halfway across the spacer between the two membranes along the path of the current flow, which here is equal to half the thickness of the spacer mesh used in the BPMED system. Because the spacer mesh reduces the open volume of the electrolyte available for ionic current conduction, we define $A_{electrolyte}$ = *geometric area* × *fraction open area*. We note that these calculations do not take into account boundary layer effects and associated concentration polarizations.[41] Thus, the analysis implicitly assumes the turbulence of the spacer mesh, flow rate, and pH gradient are sufficient to prevent significant boundary-layer effects. Further coupled fluid dynamics and migration/diffusion transport modeling of these systems will be useful as these assumptions likely break down at high current.

To obtain $\Delta\phi_{BPM}$, the $\Delta\phi_{HCl}$ and $\Delta\phi_{NaOH}$ values were subtracted from V_i-V_{ocv} measured across the reference electrodes. The term $\Delta\phi_{BPM}$ can be further broken down into the potential drop across the solid CEL and AEL ionomer electrolytes ($\Delta\phi_{CEL}$ and $\Delta\phi_{AEL}$; respectively) and η_{wd}.

$$\Delta\phi_{BPM} = \eta_{wd} + \Delta\phi_{CEL} + \Delta\phi_{AEL} \quad (4)$$

From the $\Delta\phi_{BPM}$ values, membrane conductivities, determined via H-cell measurements, and thicknesses (l) were used to calculate and subtract $\Delta\phi_{CEL}$ and $\Delta\phi_{AEL}$ to provide η_{wd}.

$$\eta_{wd} = \Delta\phi_{total,D} - \Delta\phi_{HCl} - \Delta\phi_{NaOH} - \Delta\phi_{CEL} - \Delta\phi_{AEL} \quad (5)$$

■ COMPARING PERFORMANCE VIA η_{WD}

Using the presented BPMED platform, η_{wd} was compared between the BPMED and BPMWE systems. Controlling the WD catalyst loading following the procedures described previously,[10] the catalyst loading was found to impact η_{wd} following similar trends between the two system types, where an increase in TiO_2 catalyst loading in a range of ~0−100 μg cm^{-2} led to reduced η_{wd} (Figure 3a). Similar results were found for recently reported SnO_2 nanoparticle paste catalyst (Figure 3b).[10,42]

To elucidate performance trends between the BPMWE and BPMED systems, the η_{wd} values at 0.5 A cm^{-2} were plotted versus TiO_2 catalyst loading (Figure 3c). Both the BPM water electrolysis and electrodialysis experiments revealed a characteristic U-shape observed previously with optimal TiO_2 loading of ~20 μg cm^{-2}.[10] This result suggests that advanced BPMs developed, and fundamentally understood, in a BPMWE system can be translated to more-complex systems like BPMED, allowing BPMWE systems to serve as an adequate development platform for BPMs in BPMED systems.

https://doi.org/10.1021/acsenergylett.4c03538
ACS Energy Lett. 2025, 10, 845−852

The deviations in U-shape trends seen in Figure 3c could be due to an inconsistent BPM construction at the lab-scale, impacts of co-ions from the soluble electrolytes on the physics of the BPM junction, or a difference in the static pressure on the BPM. Co-ion contaminants would increase ionic conductivity within the BPM junction, thus affecting the electric-field distribution by concentrating it more at the interfaces with AEL and CEL.[43] This could result in a weaker dependence of η_{wd} on catalyst loading, similar to what is observed when adding electrically conductive media to the BPM junction.[10] Changes in static pressure on the BPM may also lead to reduced water transport through the BPM as pressure is increased, following the trends seen in PEM electrolyzers and when determining conductivity of ion-exchange membranes.[31,32] Further, if reduced pressure leads to a less-compact BPM junction, the distance over which the electric potential drops will increase and the local electric field that is hypothesized to control water preorganization will decrease.[44] Deconvoluting these possible differences, however, is not yet possible.

We also studied a recently reported low-temperature, nano-SnO_2 paste WD catalyst. A shallower U-shape curve of η_{wd} versus loading was observed (Figure 3d).[42] Like in BPMWE, the optimal loading of the SnO_2 was higher than for TiO_2. The SnO_2 catalyst is more electrically conductive than the TiO_2 catalyst, perhaps the reason for the shallower U-shaped curve.

COMPARING BPM PERFORMANCE VIA CURRENT EFFICIENCY

Historically, production of a desired product (i.e., selectivity) was the primary goal of BPMED, but this often came at the expense of energy efficiency.[23,24] One important measure of selectivity is current efficiency. Here, current efficiency is defined as the ratio of proton (or hydroxide ion) production experimentally versus the predicted production rate at a specific current density. This generation rate (G) can be calculated using eq 6, where the current (i) passed through the system is converted to mol/s using the number of electrons transferred in the reaction (n) and Faraday's constant (F).

$$G = \frac{i}{nF} \tag{6}$$

The generation rate is then used to determine the theoretical concentration change (ΔC_{theo}) based on the amount of time (t) current was passed through the stack. The theoretical concentration change can be compared to the experimental concentration change (ΔC_{exp}), as determined via titration, as described in eqs 7−9, providing a percent current efficiency (CE).

$$\Delta C_{theo} = G \times t \tag{7}$$

$$\Delta C_{exp} = C_f - C_i \tag{8}$$

$$\frac{\Delta C_{theo}}{\Delta C_{exp}} \times 100\% = CE \tag{9}$$

We measured current efficiency using the system described above to quantify the performance of BPMs. For this, the BPMED system was held at a constant current for 30 min, with base and acid samples titrated before and after this current hold to determine the change in pH in both the acid and base reservoirs associated with the total charge passed.

Figure 4 shows the current efficiency of the BPMED system for the optimally loaded TiO_2 BPM and SnO_2 BPM, as

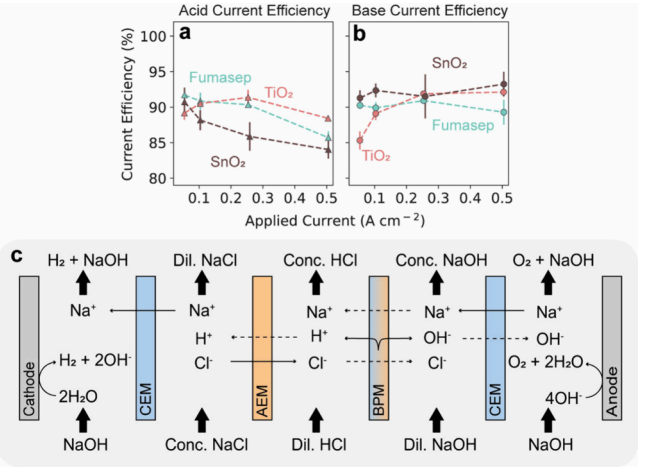

Figure 4. Current efficiency for (a) acid and (b) base production as the current is varied for a Fumasep BPM in the BPMED system (blue), TiO_2 catalyst-coated BPM (pink), and SnO_2 catalyst-coated BPM (brown). All runs were collected at 25 °C in triplicate, and error bars are shown as one standard deviation in cases where they are larger than the symbols. (c) Possible mechanisms of ion-cross over and shunting currents are represented by dashed lines in a BPMED schematic.

compared to a common commercial BPM from Fumasep. The TiO_2 BPM showed current efficiency values of ∼90% for both acid and base solutions across a current density range of 0.05−0.50 A cm^{-2}, while the SnO_2 BPM showed current efficiency values of ∼87% and 90% for acid and base, respectively (Figure 4a and 4b). A current efficiency value of ∼90% is consistent with the findings of Lucas et al., who used a similar BPMED system.[45]

Compared to Fumasep's BPM current efficiency values, the TiO_2 BPM performed slightly worse at low currents, 0.05−0.10 A cm^{-2}, and improved at higher currents, 0.25−0.50 A cm^{-2}. This trend could be due to higher flux of generated protons and hydroxide ions from the BPM junction at the higher currents, or related to the ionomer materials themselves.[46] As current increases, the efflux of proton- and hydroxide-ion mobile species likely impedes the influx of co-ions, due to concentrated ion−ion interactions, thus increasing current efficiency at higher currents.[47] This is an effect that we have previously noted, but requires further study to fully understand and engineer.[39] Lucas et al. also noted reduced current efficiency at lower currents, attributing the trend to increasing co-ion transport across the BPM at these lower currents. Similarly, the SnO_2 BPM showed similar base current efficiency trends to TiO_2, but showed a reduced acid current efficiency compared to both TiO_2 and Fumasep's BPM.

Substantial current efficiency loss can be expected given the unoptimized individual AEM and CEM that are used along with the BPM in the BPMED test platform. Because of the four-membrane configuration of this BPMED platform, current efficiency can also be reduced by ion-leakage across the supporting AEM and other two CEMs in the overall BPMED system (Figure 4b). The loss of protons across the supporting AEM, for example, can lead to reduced acid current-efficiency values. The leakage of protons is difficult to prevent, and may explain the reduced current efficiency of the acid solution at

https://doi.org/10.1021/acsenergylett.4c03538
ACS Energy Lett. 2025, 10, 845−852

high currents, compared to the basic-solution current efficiency. If the BPM ion-leakage was equivalent, then the acid and base solution current efficiencies should be the same. The optimization of the supporting AEM and CEM must be addressed in conjunction with advanced BPM integration in BPMED device cells and stacks. While the use of more-permselective membrane layers in the BPM itself might lead to further decreased co-ion crossover and thus higher current efficiencies as well, these initial findings show that the use of CELs and AELs developed for BPMWE applications can perform well in BPMED systems, especially at high-current densities.

OVERALL IMPACT OF PERFORMANCE GAINS

Compared to the commercial Fumasep BPM, both the TiO_2 and SnO_2 catalyzed BPMs performed dramatically better with respect to energy consumption (Figure 5a), with a nearly two-fold decrease in energy consumption for the production of H^+ or OH^- product. Furthermore, the durability of the SnO_2 catalyzed BPM is improved over the Fumasep BPM in the BPMED system tested, with Fumasep showing a degradation of ~2.1 mV h^{-1} and SnO_2 showing a degradation of ~0.3 mV h^{-1} (Figure 5b). With these improvements, the catalyzed BPM can operate at higher current densities, while also providing higher product output at competitive efficiencies without compromising durability. These improvements may enable electrochemical stack systems to overcome economic barriers in applications like CO_2 electrolysis and brine remediation. However, detailed and application-specific techno-economic analyses are required to fully understand the impact of catalyzed BPMs on the viability of BPM containing technologies.

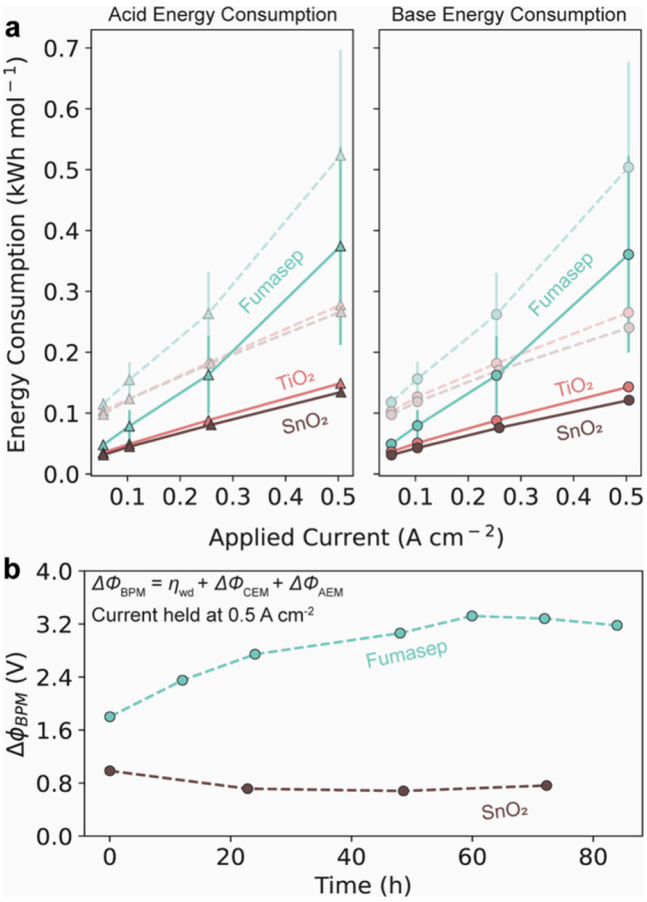

Figure 5. (a) Energy consumption of commercial Fumasep, TiO_2, and SnO_2 BPMs in the BPMED system for the production of either H^+ (acid) or OH^- (base) plotted versus applied current. The energy consumption for a single repeating cell in the overall stack is represented as solid, bold lines, while the total stack containing a single cell is represented as dashed, faded lines. Data collected in triplicate with error bars shown as one standard deviation in cases where they are larger than the symbols. (b) BPM transmembrane potential ($\Delta\phi_{BPM}$) versus time for commercial Fumasep and SnO_2 catalyzed BPM held at 0.5 A cm^{-2} in the BPM electrodialysis system. All runs were collected at 25 °C.

CONCLUSION

We reported the initial translation of advanced, catalyzed BPMs from membrane-electrode assemblies to BPMED systems, showing that metal-oxide catalysts optimized in one system also improves performance in the other. The new catalyzed BPM provided current efficiency values for acid–base generation that exceeded those found for common commercial Fumasep BPM at current-densities above 0.20 A cm^{-2}, while requiring only roughly half of the driving voltage across the BPM. We also report a simple design for BPMED test platform that allows for the isolation of electrostatic potential drops across individual membranes in the system, allowing for the measurement of important characteristics like η_{wd} within the BPMED system. While further research is required to better understand the impacts of compression and possible co-ion fouling mechanisms in BPMWE-based BPM, the increased current densities in part enabled by the advanced BPMs are expected to facilitate broader adoption of BPM-based electrochemical technologies in electrodialysis-type platforms.

ASSOCIATED CONTENT

Supporting Information

The Supporting Information is available free of charge at https://pubs.acs.org/doi/10.1021/acsenergylett.4c03538.

Membranes and catalysts; advanced BPM fabrication; assembly of electrodialysis system with schematic illustrations; standard operating procedure for BMPED at Figshare: 10.6084/m9.figshare.28021250.v1; CAD and 3D printing files of BPMED system components at Figshare: 10.6084/m9.figshare.28021196.v1; laser cutting files for gaskets and spacer mesh at Figshare: 10.6084/m9.figshare.28021217.v1; procedure for data collection (electrochemical, polarization-curve, and current efficiency data) and corresponding LabView files at Figshare: 10.6084/m9.figshare.28021223.v1; determination of BPMED circuits $A_{electrolyte}$; titration of acid and base solutions; assembly of system for leak testing; determination of Nafion and Versogen conductivity; calculations for assessing energy consumption; procedure for stability test, post-mortem assessment of SnO_2 BPM from stability test with EDS line scan data; and comparison of total cell potential. (PDF)

AUTHOR INFORMATION

Corresponding Author

Shannon W. Boettcher – *Oregon Center for Electrochemistry, Department of Chemistry and Biochemistry, University of Oregon, Eugene, Oregon 97403, United States; Department*

https://doi.org/10.1021/acsenergylett.4c03538
ACS Energy Lett. 2025, 10, 845–852

of Chemical & Biomolecular Engineering and Department of Chemistry, University of California, Berkeley, California 94720, United States; Energy Storage and Distributed Resources Division, Lawrence Berkeley National Laboratory, Berkeley, California 94720, United States; orcid.org/0000-0001-8971-9123; Email: boettcher@berkeley.edu

Authors

Olivia T. Vulpin − *Oregon Center for Electrochemistry, Department of Chemistry and Biochemistry, University of Oregon, Eugene, Oregon 97403, United States*

James B. Mitchell − *Oregon Center for Electrochemistry, Department of Chemistry and Biochemistry, University of Oregon, Eugene, Oregon 97403, United States*

Lihaokun Chen − *Oregon Center for Electrochemistry, Department of Chemistry and Biochemistry, University of Oregon, Eugene, Oregon 97403, United States*

Jeonghoon Lim − *Energy Storage and Distributed Resources Division, Lawrence Berkeley National Laboratory, Berkeley, California 94720, United States*

Sayantan Sasmal − *Oregon Center for Electrochemistry, Department of Chemistry and Biochemistry, University of Oregon, Eugene, Oregon 97403, United States*

Nathan G. Price − *Oregon Center for Electrochemistry, Department of Chemistry and Biochemistry, University of Oregon, Eugene, Oregon 97403, United States*

Sam R. Jarvis − *Oregon Center for Electrochemistry, Department of Chemistry and Biochemistry, University of Oregon, Eugene, Oregon 97403, United States*

Complete contact information is available at: https://pubs.acs.org/10.1021/acsenergylett.4c03538

Notes

The authors declare the following competing financial interest(s): The authors have filed a provisional patent application on materials reported in this manuscript and are working to commercialize advanced BPMs.

■ ACKNOWLEDGMENTS

This work on BPMED was funded by ARPA-E grant DE-AR0001540. Preliminary work central to this project studying advanced BPM response in contact with electrolytes was completed with support U.S. Advanced Research Projects Agency-Energy (ARPA-E), grant DE-AR0001502. The work made use of shared instrumentation in the Center for Advanced Materials Characterization in Oregon (CAMCOR) and the Phil and Penny Knight Campus for Accelerating Scientific Impact.

■ REFERENCES

(1) Pärnamäe, R.; Mareev, S.; Nikonenko, V.; Melnikov, S.; Sheldeshov, N.; Zabolotskii, V.; Hamelers, H. V. M.; Tedesco, M. Bipolar Membranes: A Review on Principles, Latest Developments, and Applications. *J. Membr. Sci.* **2021**, *617*, No. 118538.

(2) Ge, Z.; Shehzad, M. A.; Yang, X.; Li, G.; Wang, H.; Yu, W.; Liang, X.; Ge, X.; Wu, L.; Xu, T. High-Performance Bipolar Membrane for Electrochemical Water Electrolysis. *J. Membr. Sci.* **2022**, *656*, No. 120660.

(3) Giesbrecht, P. K.; Freund, M. S. Recent Advances in Bipolar Membrane Design and Applications. *Chem. Mater.* **2020**, *32* (19), 8060−8090.

(4) Zhang, Y.; Yu, D.; Jia, C.; Sun, L.; Tong, A.; Wang, Y.; Wang, Y.; Huang, L.; Tang, J. Advances and Promotion Strategies of Membrane-Based Methods for Extracting Lithium from Brine. *Desalination* **2023**, *566*, 116891−116891.

(5) Yang, Y.; Gao, X.; Fan, A.; Fu, L.; Gao, C. An Innovative Beneficial Reuse of Seawater Concentrate Using Bipolar Membrane Electrodialysis. *J. Membr. Sci.* **2014**, *449*, 119−126.

(6) Fernandez-Gonzalez, C.; Dominguez-Ramos, A.; Ibañez, R.; Irabien, A. Electrodialysis with Bipolar Membranes for Valorization of Brines. *Sep. Purif. Rev.* **2016**, *45* (4), 275−287.

(7) Lim, A.; Kim, H.; Henkensmeier, D.; Jong Yoo, S.; Young Kim, J.; Young Lee, S.; Sung, Y.; Jang, J. H.; Park, H. S. A Study on Electrode Fabrication and Operation Variables Affecting the Performance of Anion Exchange Membrane Water Electrolysis. *J. Ind. Eng. Chem.* **2019**, *76*, 410−418.

(8) Mason, T. J.; Millichamp, J.; Neville, T. P.; Shearing, P. R.; Simons, S.; Brett, D. J. L. A Study of the Effect of Water Management and Electrode Flooding on the Dimensional Change of Polymer Electrolyte Fuel Cells. *J. Power Sources* **2013**, *242*, 70−77.

(9) Kulkarni, N.; Cho, J. I. S.; Jervis, R.; Roberts, E. P. L.; Francesco, I.; Kok, M. D. R.; Shearing, P. R.; Brett, D. J. L. The Effect of Non-Uniform Compression on the Performance of Polymer Electrolyte Fuel Cells. *J. Power Sources* **2022**, *521*, No. 230973.

(10) Chen, L.; Xu, Q.; Oener, S. Z.; Fabrizio, K.; Boettcher, S. W. Design Principles for Water Dissociation Catalysts in High-Performance Bipolar Membranes. *Nat. Commun.* **2022**, *13* (1), 3846.

(11) Krivina, R. A.; Lindquist, G. A.; Yang, M. C.; Cook, A. K.; Hendon, C. H.; Motz, A. R.; Capuano, C.; Ayers, K. E.; Hutchison, J. E.; Boettcher, S. W. Three-Electrode Study of Electrochemical Ionomer Degradation Relevant to Anion-Exchange-Membrane Water Electrolyzers. *ACS Appl. Mater. Interfaces* **2022**, *14* (16), 18261−18274.

(12) Oener, S. Z.; Foster, M. J.; Boettcher, S. W. Accelerating Water Dissociation in Bipolar Membranes and for Electrocatalysis. *Science* **2020**, *369*, 1099−1103.

(13) Bui, J. C.; Lees, E. W.; Marin, D.; Stovall, T. N.; Chen, L.; Kusoglu, A.; Nielander, A. C.; Jaramillo, T. F.; Boettcher, S. W.; Bell, A. T.; et al. Multi-Scale Physics of Bipolar Membranes in Electrochemical Processes. *Nat. Chem. Eng.* **2024**, *1* (1), 45−60.

(14) Strathmann, H.; Krol, J. J.; Rapp, H.-J.; Eigenberger, G. Limiting Current Density and Water Dissociation in Bipolar Membranes. *J. Membr. Sci.* **1997**, *125*, 123−142.

(15) Simons, R. Strong Electric Field Effects on Proton Transfer between Membrane-Bound Amines and Water. *Nature* **1979**, *280*, 824−826.

(16) Mafé, S.; Ramírez, P. Electrochemical Characterization of Polymer Ion-Exchange Bipolar Membranes. *Acta Polym.* **1997**, *48* (7), 234−250.

(17) Hurwitz, H. D.; Dibiani, R. Experimental and Theoretical Investigations of Steady and Transient States in Systems of Ion Exchange Bipolar Membranes. *J. Membr. Sci.* **2004**, *228* (1), 17−43.

(18) Blommaert, M. A.; Aili, D.; Tufa, R. A.; Li, Q.; Smith, W. A.; Vermaas, D. A. Insights and Challenges for Applying Bipolar Membranes in Advanced Electrochemical Energy Systems. *ACS Energy Lett.* **2021**, *6* (7), 2539−2548.

(19) Simons, R.; Khanarian, G. Water Dissociation in Bipolar Membranes Experiments and Theory. *J. Membr. Biol.* **1978**, *38*, 11−30.

(20) Lovrecek, B.; Kunst, B. Electrochemical Properties of the Ion-Exchange Membranes Junction. I. *Croat. Chem. Acta* **1962**, *34* (3), 137−151.

(21) Chen, Y.; Martínez, R. J.; Gervasio, D.; Baygents, J. C.; Farrell, J. Water Splitting Promoted by Electronically Conducting Interlayer Material in Bipolar Membranes. *J. Appl. Electrochem.* **2020**, *50* (1), 33−40.

(22) Chen, Y.; Wrubel, J. A.; Klein, W. E.; Kabir, S.; Smith, W. A.; Neyerlin, K. C.; Deutsch, T. G. High-Performance Bipolar Membrane Development for Improved Water Dissociation. *ACS Appl. Polym. Mater.* **2020**, *2* (11), 4559−4569.

(23) Espinoza, C.; Kitto, D.; Kamcev, J. Counter-Ion Conductivity and Selectivity Trade-Off for Commercial Ion-Exchange Membranes

at High Salinities. *ACS Appl. Polym. Mater.* **2023**, *5* (12), 10324−10333.
(24) Kim, Y.; Walker, W. S.; Lawler, D. F. Competitive Separation of Di- Vs. Mono-Valent Cations in Electrodialysis: Effects of the Boundary Layer Properties. *Water Res.* **2012**, *46* (7), 2042−2056.
(25) Huang, C.; Xu, T. Electrodialysis with Bipolar Membranes for Sustainable Development. *Environ. Sci. Technol.* **2006**, *40*, 5233−5243.
(26) Strathmann, H. *Ion-Exchange Membrane Separation Processes*. Elsevier, 2004, Vol. *9*, 287−330.
(27) Zhang, Y.-n.; Yu, D.-h.; Jia, C.-y.; Sun, L.-y.; Tong, A.; Wang, Y.; Wang, Y.-x.; Huang, L.-j.; Tang, J.-g Advances and Promotion Strategies of Membrane-Based Methods for Extracting Lithium from Brine. *Desalination* **2023**, *566*, 116891−116891.
(28) Zhang, Z. B. Low-Temperature Electrochemical Cement Clinker Production. *ACS Energy Lett.* **2023**, *8* (9), 3927−3934.
(29) Xu, Q.; Oener, S. Z.; Lindquist, G.; Jiang, H.; Li, C.; Boettcher, S. W. Integrated Reference Electrodes in Anion-Exchange-Membrane Electrolyzers: Impact of Stainless-Steel Gas-Diffusion Layers and Internal Mechanical Pressure. *ACS Energy Lett.* **2021**, *6* (2), 305−312.
(30) Bender, G.; Carmo, M.; Smolinka, T.; Gago, A.; Danilovic, N.; Mueller, M.; Ganci, F.; Fallisch, A.; Lettenmeier, P.; Friedrich, K. A.; et al. Initial Approaches in Benchmarking and Round Robin Testing for Proton Exchange Membrane Water Electrolyzers. *Int. J. Hydrogen Energy* **2019**, *44* (18), 9174−9187.
(31) Stähler, M.; Stähler, A.; Scheepers, F.; Carmo, M.; Lehnert, W.; Stolten, D. Impact of Porous Transport Layer Compression on Hydrogen Permeation in PEM Water Electrolysis. *Int. J. Hydrogen Energy* **2020**, *45* (7), 4008−4014.
(32) Yun, S.-H.; Shin, S.-H.; Lee, J.-Y.; Seo, S.-J.; Oh, S.; Choi, Y.-W.; Moon, S. H. Effect of Pressure on through-Plane Proton Conductivity of Polymer Electrolyte Membranes. *J. Membr. Sci.* **2012**, *417*, 210−216.
(33) Gurreri, L.; Tamburini, A.; Cipollina, A.; Micale, G.; Ciofalo, M. Flow and Mass Transfer in Spacer-Filled Channels for Reverse Electrodialysis: A CFD Parametrical Study. *J. Membr. Sci.* **2016**, *497*, 300−317.
(34) Campione, A.; Gurreri, L.; Ciofalo, M.; Micale, G.; Tamburini, A.; Cipollina, A. Electrodialysis for Water Desalination: A Critical Assessment of Recent Developments on Process Fundamentals, Models and Applications. *Desalination* **2018**, *434*, 121−160.
(35) Fehér, J.; Keslerová, K.; Amrich, M. A Tool for a Spacer Material and Ion-Exchange Membrane Compatibility Evaluation for Electrodialysis Module Design. *Period. Polytech., Chem. Eng.* **2018**, *62* (2), 144−149.
(36) Kim, Y.; Walker, W. S.; Lawler, D. F. Electrodialysis with Spacers: Effects of Variation and Correlation of Boundary Layer Thickness. *Desalination* **2011**, *274* (1−3), 54−63.
(37) Pourcelly, G. Electrodialysis with Bipolar Membranes Principles, Optimization, and Applications. *J. Electrochem.* **2002**, *38* (8), 919−926.
(38) Strathmann, H. Electrodialysis, a Mature Technology with a Multitude of New Applications. *Desalination* **2010**, *264* (3), 268−288.
(39) Marin, D. H.; Perryman, J. T.; Hubert, M. A.; Lindquist, G. A.; Chen, L.; Aleman, A. M.; Kamat, G. A.; Niemann, V. A.; Stevens, M. B.; Regmi, Y. N.; et al. Hydrogen Production with Seawater-Resilient Bipolar Membrane Electrolyzers. *Joule* **2023**, *7* (4), 765−781.
(40) *CRC Handbook of Chemistry and Physics*; CRC Press, 2014.
(41) Vermaas, D. A.; Wiegman, S.; Nagaki, T.; Smith, W. A. Ion Transport Mechanisms in Bipolar Membranes for (Photo)-Electrochemical Water Splitting. *Sustain. Energy Fuels* **2018**, *2* (9), 2006−2015.
(42) Sasmal, S.; Chen, L.; Sarma, P. V.; Vulpin, O. T.; Simons, C. R.; Wells, K. M.; Spontak, R. J.; Boettcher, S. W. Materials Descriptors for Advanced Water Dissociation Catalysts in Bipolar Membranes. *Nat. Mater.* **2024**, *23* (10), 1421−1427.
(43) Toh, W. L.; Dinh, H. Q.; Chu, A. T.; Sauvé, E. R.; Surendranath, Y. The Role of Ionic Blockades in Controlling the Efficiency of Energy Recovery in Forward Bias Bipolar Membranes. *Nat. Energy* **2023**, *8* (12), 1405−1416.
(44) Chen, L.; Xu, Q.; Boettcher, S. W. Kinetics and Mechanism of Heterogeneous Voltage-Driven Water-Dissociation Catalysis. *Joule* **2023**, *7* (8), 1867−1886.
(45) Lucas, É.; Han, L.; Sullivan, I.; Atwater, H. A.; Xiang, C. Measurement of Ion Transport Properties in Ion Exchange Membranes for Photoelectrochemical Water Splitting. *Front. Energy Res.* **2022**, *10*, No. 1001684.
(46) Parnamae, R.; Tedesco, M.; Wu, M.-C.; Hou, C.-H.; Hamelers, H. V.M.; Patel, S. K.; Elimelech, M.; Biesheuvel, P.M.; Porada, S. Origin of Limiting and Overlimiting Currents in Bipolar Membranes. *Environ. Sci. Technol.* **2023**, *57* (26), 9664−9674.
(47) Newman, J.; Bennion, D.; Tobias, C. W. Mass Transfer in Concentrated Binary Electrolytes. *Ber. Bunsen-Ges. Phys. Chem.* **1965**, *69* (7), 608−612.

https://doi.org/10.1021/acsenergylett.4c03538
ACS Energy Lett. 2025, 10, 845−852